Geochemistry, Geophysics, Geosystems

Supporting Information for

Thermal evolution of asymmetric hyperextended magma-poor rift systems: results from numerical modelling and Pyrenean field observations

Rodolphe Lescoutre[1], Julie Tugend[1,2,3], Sascha Brune[4,5], Emmanuel Masini[3], Gianreto Manatschal[1]

[1]IPGS, EOST-CNRS, Université de Strasbourg, Strasbourg, France

[2]Sorbonne Université, CNRS-INSU, Institut des Sciences de la Terre Paris, ISTeP UMR 7193, F-75005 Paris, France.

[3]Total R&D, CSTJF, Pau, France

[4]GFZ Potsdam, German Research Centre for Geosciences, Potsdam, Germany

[5]Institute of Earth and Environmental Sciences, University of Potsdam, Germany

Contents of this file

Additional Supporting Information (Files uploaded separately)

Summary

This supporting information file contains the parameters used for the numerical model (Table S1). The same numerical model is run with moderate and high sedimentation rates and depicted in Figure S2. Movie S3 shows the complete evolution of the numerical model of asymmetric rifting and the evolution of topography and top basement heat flow from where are extracted the 3 snapshots of Figure 3. We include new vitrinite reflectance data from the Arzacq-Mauléon basin in Figure S5 and compile the full data sets of RSCM data (Table S4) available in the literature for the Mauléon-Arzacq basin. The Table S6 show the vitrinite reflectance (%VR) values from the boreholes converted in T_{max} based on the formulas proposed by Barker (1988) and Barker & Pawlewicz (1994).

Movie S3. Numerical model of asymmetric rifting and top basement heat flow evolution.

Table S4. RSCM datasets compiled for this study. Longitudes (x) and latitudes (y) are in Lambert 93 coordinate system (in meters).

Table S6. Conversion of %VR from the Mauléon basin to T_{max}.

Parameter	**Upper Crust**	**Lower Crust**	**Strong Mantle**	**Weak Mantle**
Density, ρ (kg m^{-3})	2700	2850	3280	3300
Thermal expansivity, α_T (10^{-5} K^{-1})	2.7	2.7	3.0	3.0
Bulk modulus, K (GPa)	55	63	122	122
Shear modulus, G (GPa)	36	40	74	74
Heat capacity, C_p (J kg^{-1} K^{-1})	1200	1200	1200	1200
Heat conductivity, λ (W K^{-1} m^{-1})	2.5	2.5	3.3	3.3
Radiogenic heat production, A (μW m^{-3})	1.5	0.2	0.0	0.0
Initial friction coefficient, μ (-)	0.5	0.5	0.5	0.5
Cohesion, c (MPa)	5.0	5.0	5.0	5.0
Pre-exponential constant for diffusion creep, log(B_{Diff}) (Pa^{-1} s^{-1})	-	-	-8.65	-8.66
Activation energy for diffusion creep, E_{Diff} (kJ / mol)	-	-	375	335
Activation volume for diffusion creep, V_{Diff} (cm^{-3} / mol)	-	-	6	4
Pre-exponential constant for dislocation creep, log(B_{Disloc}) (Pa^{-n}s^{-1})	-28.00	-15.40	-15.56	-15.05
Power law exponent for dislocation creep, n	4.0	3.0	3.5	3.5
Activation energy for dislocation creep, E_{Disloc} (kJ / mol)	223	356	530	480
Activation volume for dislocation creep, V_{Disloc} (cm^{-3}/mol)	0	0	13	10

Table S1. Thermo-mechanical parameters. During frictional and viscous strain softening, μ and B_{Disloc} respectively vary linearly for brittle and viscous strain between 0 and 1. For strains larger than 1, they remain constant. We thereby use a minimum friction coefficient of 0.05 and a maximum pre-exponential factor that is 30 times larger than the listed value, representing a modest viscosity decrease between 0.3 and 0.4 if compared to unstrained material (Brune et al., 2014). We mimic the heterogeneous distribution of faults by randomizing the initial strain distribution between values of 0 and 0.2, which results in an initial spread of friction coefficients between 0.4 and 0.5.

a)

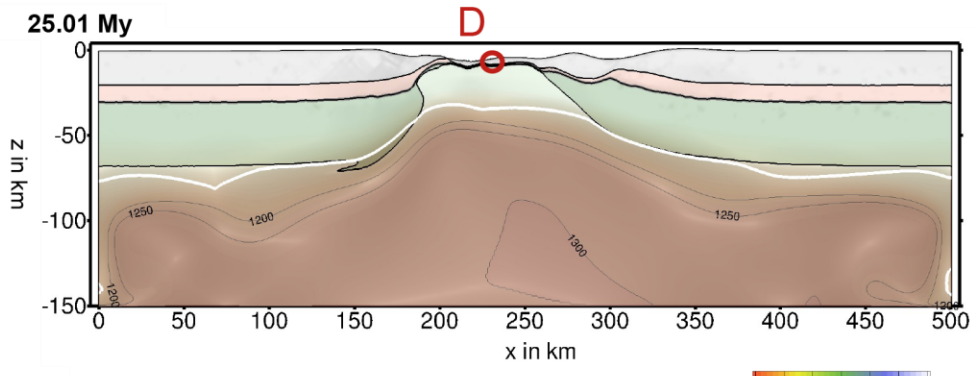
25.01 My
D
z in km
x in km
0
-50
-100
-150
0
50
100
150
200
250
300
350
400
450
500
1250
1200
1300

b)

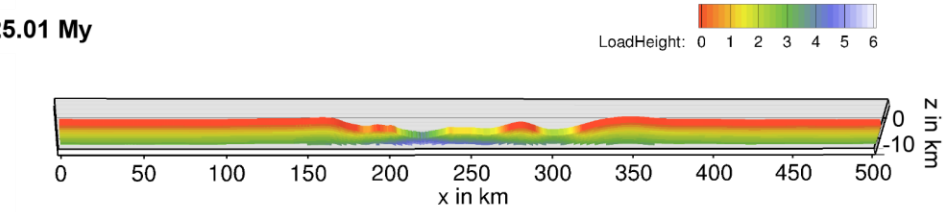
25.01 My
LoadHeight: 0 1 2 3 4 5 6
z in km
x in km
0
-10
0
50
100
150
200
250
300
350
400
450
500

c)

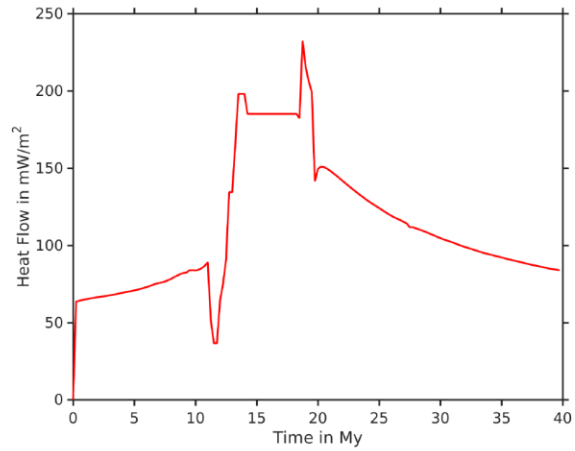
Heat Flow in mW/m^2
Time in My
0
50
100
150
200
250
0
5
10
15
20
25
30
35
40

d)

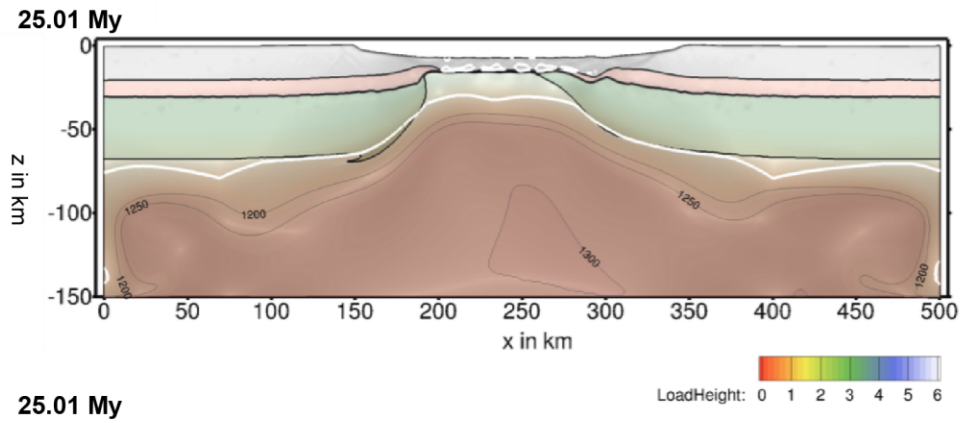
25.01 My
z in km
x in km
0
-50
-100
-150
0
50
100
150
200
250
300
350
400
450
500
1250
1200
1300

e)

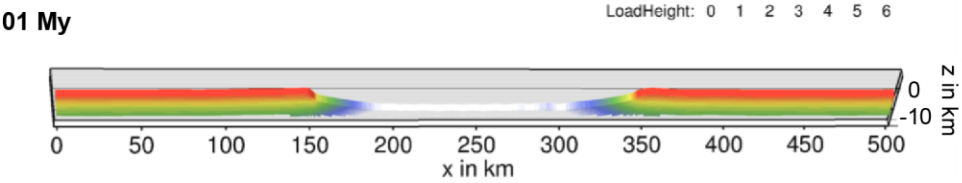
25.01 My
LoadHeight: 0 1 2 3 4 5 6
z in km
x in km
0
-10
0
50
100
150
200
250
300
350
400
450
500

Figure S2. Role of sediments on the mode of deformation. a) The model is identical to the setup shown in Figure 3 and Movie S3 but here we add sediments at each step in a way that the basin is always filled to 3 km below the surface (moderate sedimentation rate). The thermal gradient in the sediments is set to 80°C/km. The model shows similar brittle asymmetric deformation. b) Sediment thickness (LoadHeight in km) is represented along the aborted rift system at 25My. Note that the deepest part (upper-lower plate transition) records about 4.5 km of sediments during rifting. c) Heat flow evolution of marker D (see location at the end of rifting on a)). d) In this model, the sediments are filled to 1 km below the surface at each time increment (very high sedimentation rate). The thermal gradient in sediments is also fixed at 80°C/km. The deformation appears more ductile (crustal boudins and smooth to flat top basement geometry) and the rift is roughly symmetric. e) Sediment thickness at the end of rifting for the very high sedimentation rate with more than 6 km of sedimentations in the deepest part. We conclude that for moderate sedimentation rate the shape of the heat flow evolution and the crustal deformation is similar to the model without sediments, however, maximum heat flow remains high for much longer. For very high sedimentation rate, the crustal deformation is more symmetric and ductile mode of deformation prevails.

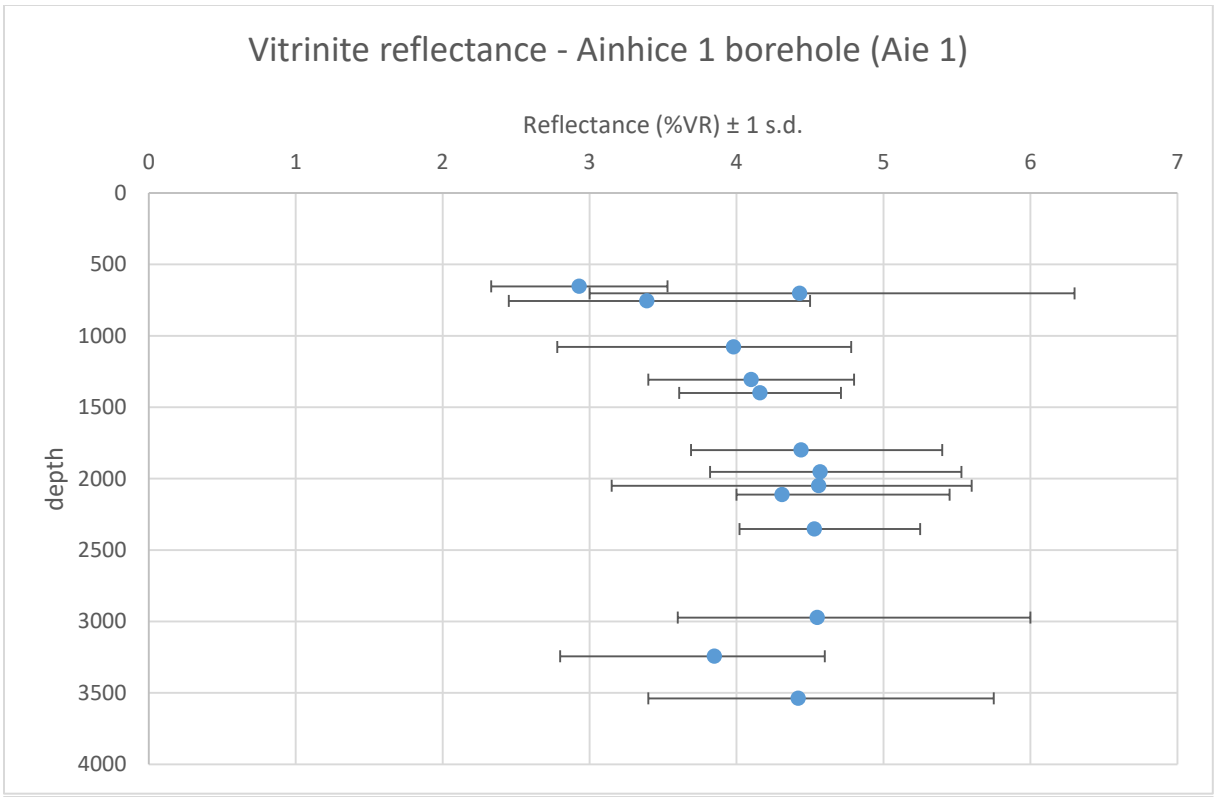

75

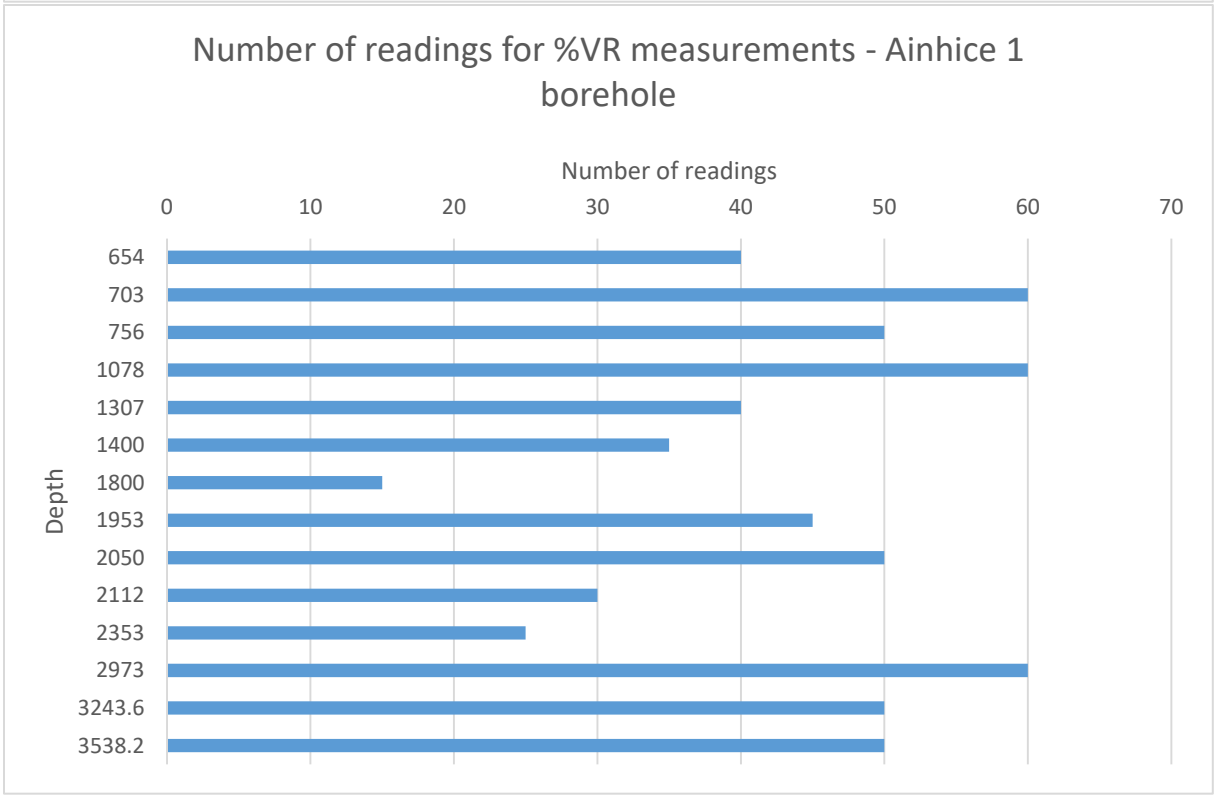

76

77 **Figure S5.** See caption on page 13.

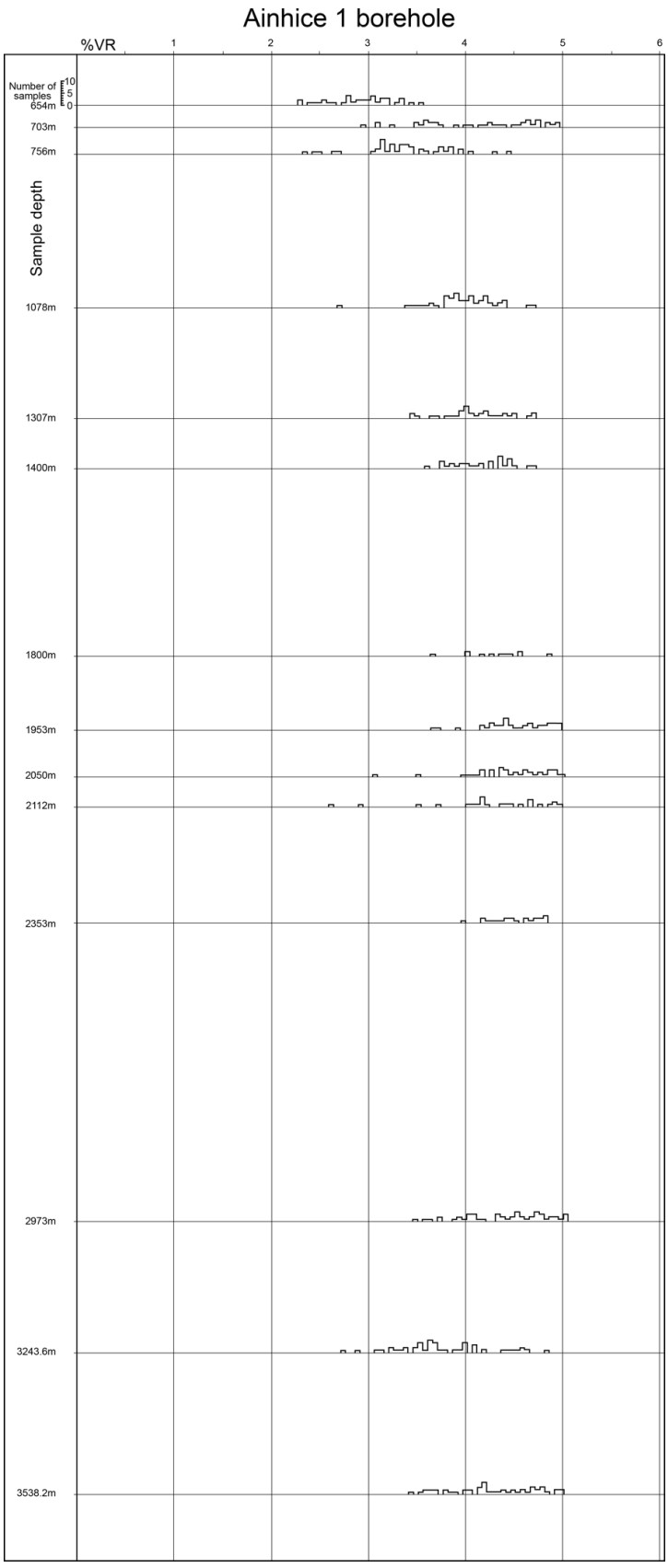

Figure S5. See caption on page 13.

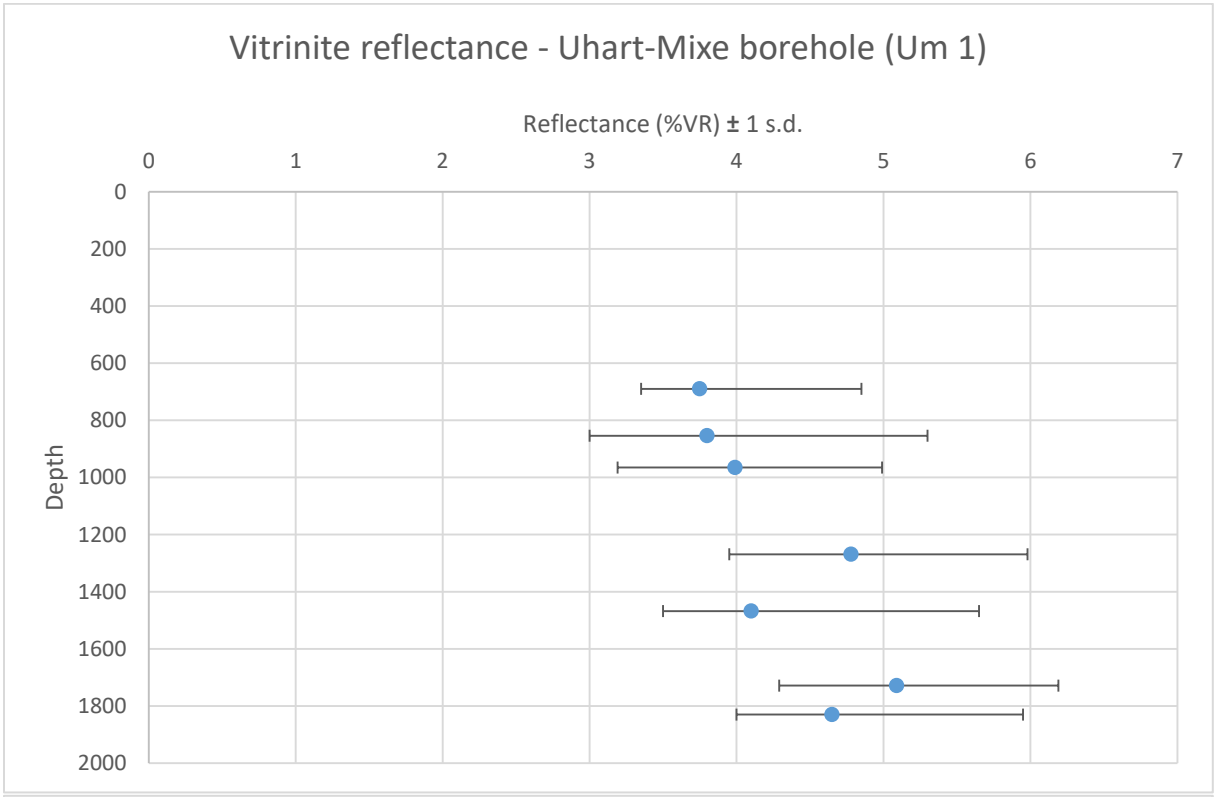

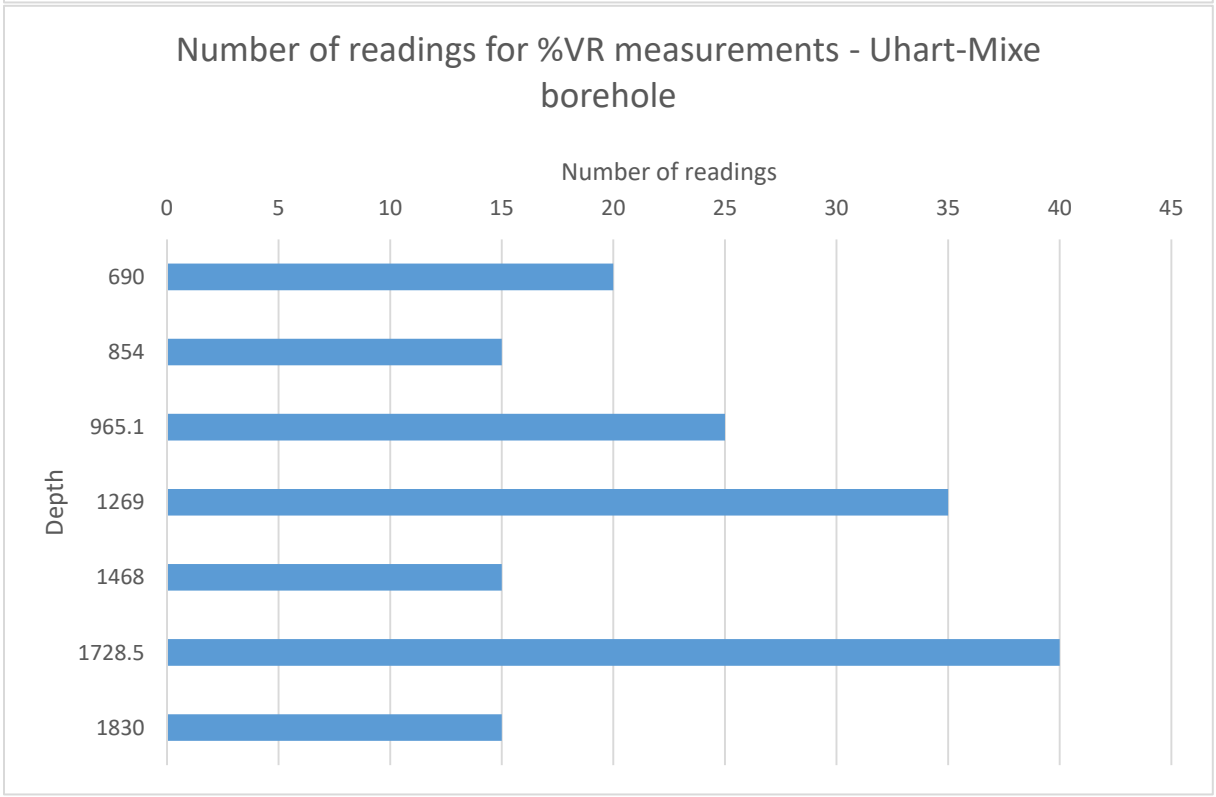

Figure S5. See caption on page 13.

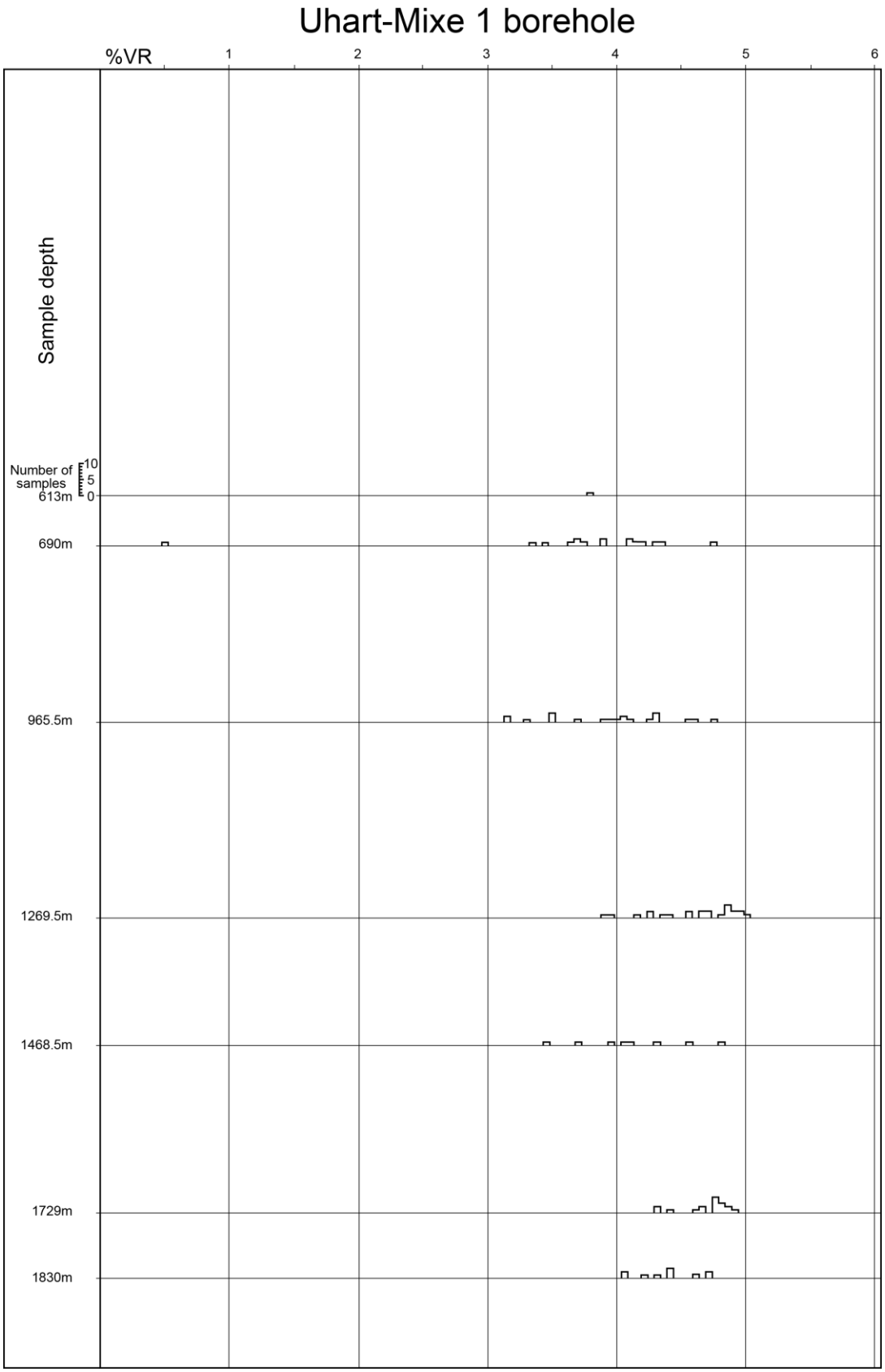

Figure S5. See caption on page 13.

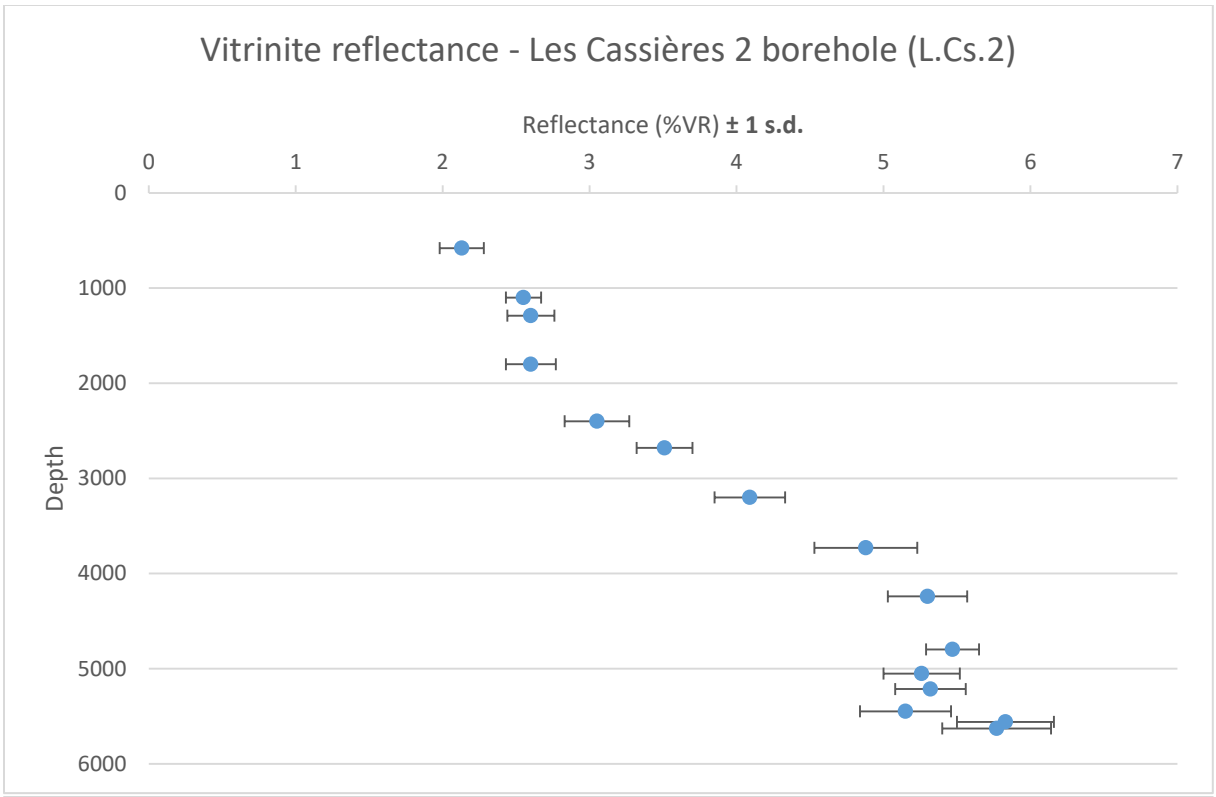

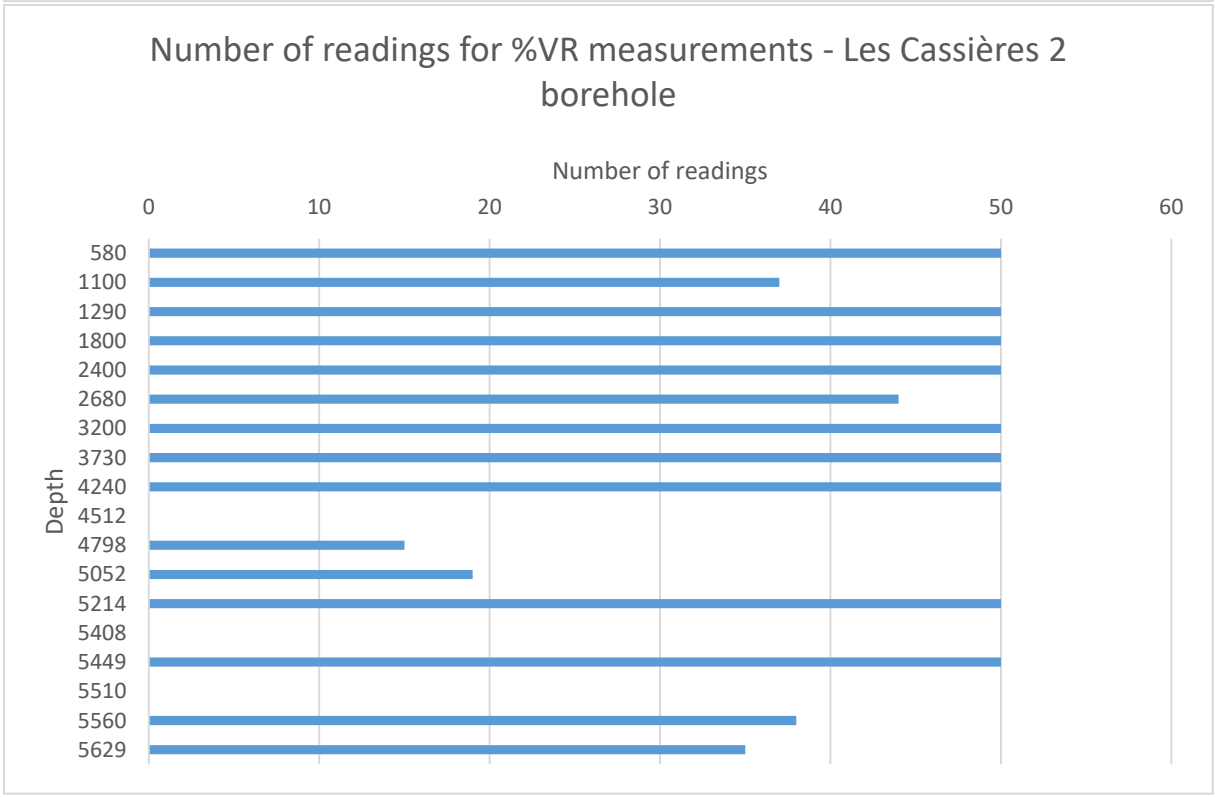

Figure S5. See caption on page 13.

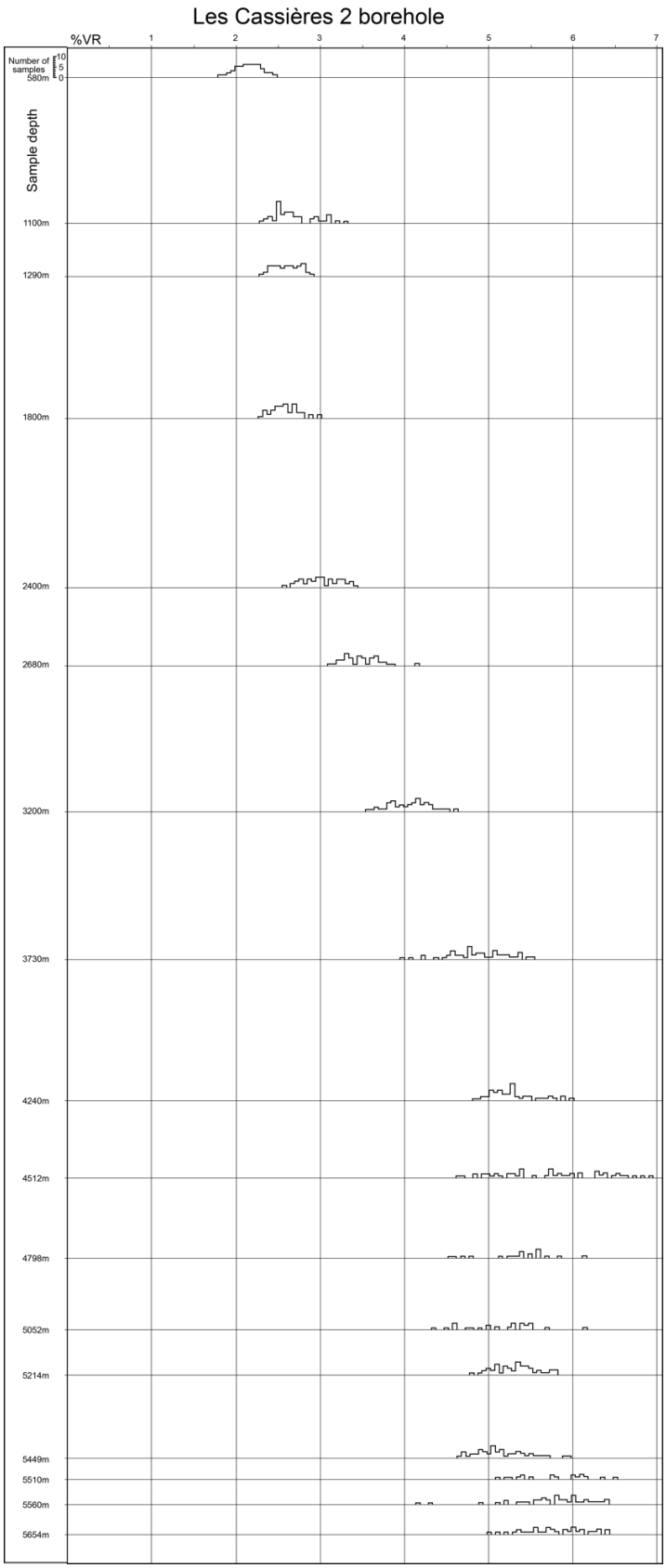

Figure S5. See caption on page 13.

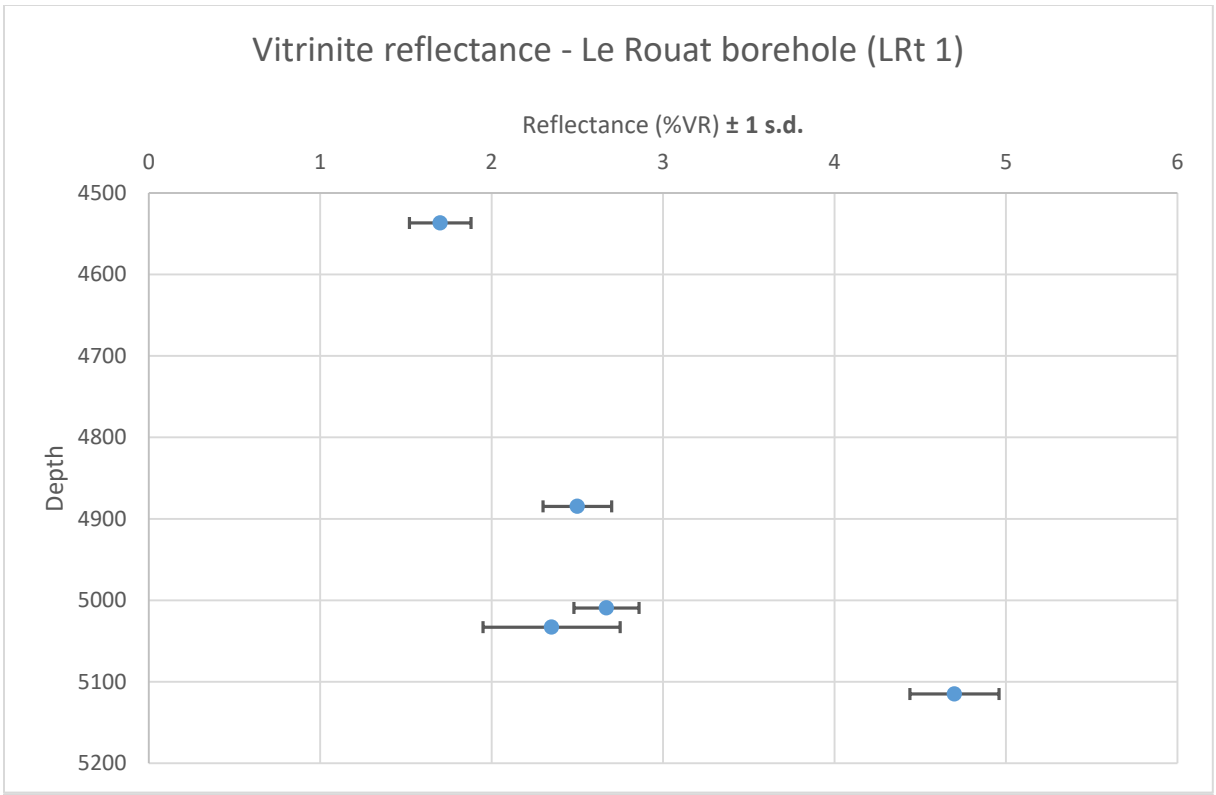

92

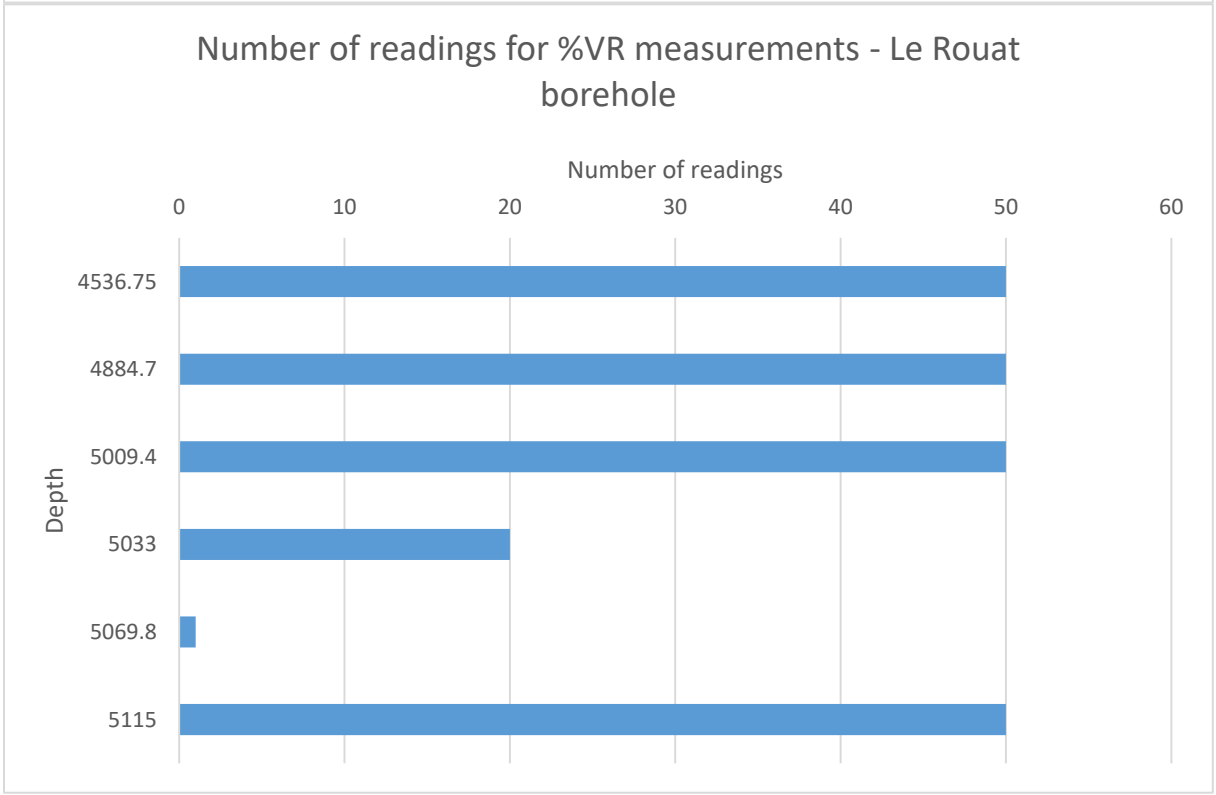

93

94 **Figure S5.** See caption on page 13.

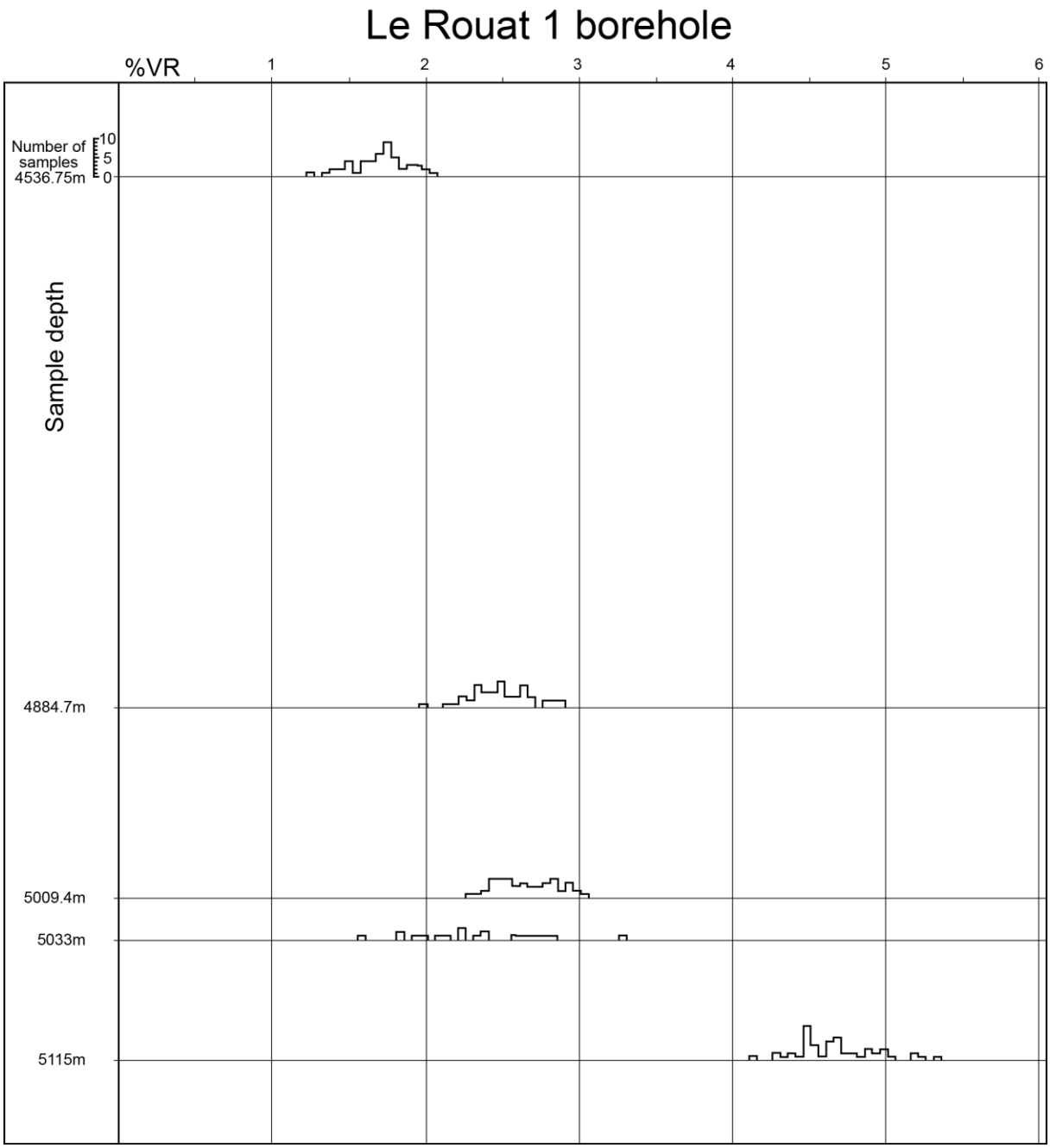

Figure S5. Vitrinite reflectance data from the Arzacq-Mauléon basin (courtesy of Total). The measurements for each depth and the number of samples are shown. We also present the histograms provided by the Total company.